THE JOURNAL OF BIOLOGICAL CHEMISTRY
Vol. 278, No. 30, Issue of July 25, pp. 27966–27970, 2003

Printed in U.S.A.

Crystal Structure of the Ectodomain of Human FcαRI*

Received for publication, May 27, 2003, and in revised form, June 3, 2003
Published, JBC Papers in Press, June 3, 2003, DOI 10.1074/jbc.C300223200

Yi Ding‡§¶, Gang Xu¶‖, Maojun Yang‡¶‖, Min Yao, George F. Gao‡§, Linfang Wang‖, Wei Zhang‖‡‡, and Zihe Rao‡§ §§**

*From the ‡Ministry of Education Protein Science Laboratory & Laboratory of Structural Biology, Tsinghua University, Beijing, 100084, China, the ‖Institute of Basic Medical Sciences, Chinese Academy of Medical Sciences, Peking Union Medical College, 5 Dong Dan San Tiao, Beijing 100005, China, the §Institute of Biophysics, Chinese Academy of Science, Beijing 100101, China, and the **Division of Biological Sciences, Graduate School of Science, Hokkaido University, 060-0810 Sapporo, Japan*

Human FcαRI (CD89) is the receptor specific for IgA, an immunoglobulin that is abundant in mucosa and is also found in high concentrations in serum. Although FcαRI is an immunoglobulin Fc receptor (FcR), it differs in many ways from FcRs for other immunoglobulin classes. The genes of most FcRs are located on chromosome 1 at 1q21–23, whereas FcαRI is on chromosome 19, at 19q13.4, a region called the leukocyte receptor complex, because it is clustered with several leukocyte receptor families including killer cell inhibitory receptors (KIRs) and leukocyte Ig-like receptors (LIRs). The amino acid sequence of FcαRI shares only 20% homology with other FcRs but it has around 35% homology with its neighboring LIRs and KIRs. In this work, we analyzed the crystal structure of the ectodomain of FcαRI and examined structure similarities between FcαRI and KIR2DL1, KIR2DL2 and LIR-1. Our data show that FcαRI, KIRs, and LIRs share a common hydrophobic core in their interdomain interface, and FcαRI is evolutionally closer to LIR than KIR.

In humans, IgA is the most abundant immunoglobulin in secretions, and it constitutes about 20% of the immunoglobulin pool in serum (1, 2). Since its turnover rate is faster than other immunoglobulins, the daily production of IgA exceeds all other immunoglobulins combined (3). Undoubtedly, IgA should to play important roles in immune defense against invaded pathogens.

Five types of IgA receptors have been recognized so far. They are FcαRI (CD89), the polymeric Ig receptor, Fcα/μR, the transferrin receptor, and the asialoglycoprotein receptor (1). Among them, FcαRI is the only one that specifically binds IgA. On ligation of IgA complexed with antigens, FcαRI is able to mediate various cellular responses including phagocytosis, antibody-dependent cell cytotoxicity, oxidative bursts, and release of inflammatory mediators (1).

FcαRI belongs to the immunoglobulin superfamily and contains an extracellular region of 206 amino acids, a transmembrane domain of 19 amino acids and a cytoplasmic region of 41 amino acids (4). The extracellular region of FcαRI consists of two Ig-like domains, EC1 and EC2, and six potential sites for *N*-glycosylation. The receptor binds IgA1 and IgA2 with an equal affinity (5). A number of residues including Tyr^{35}, Arg^{52}, Tyr^{81}, Arg^{82}, Ile^{83}, Gly^{84}, His^{85}, and Tyr^{86} on FcαRI are potentially involved in IgA binding (6, 7).

Although FcαRI is an immunoglobulin Fc receptor (FcR),[1] it differs in many ways with FcRs for other immunoglobulin classes. IgG receptor FcγRIII and IgE receptor FcϵRI bind antibodies in the near hinge regions and form 1:1 complexes (8, 9), whereas FcαRI binds the C_H2-C_H3 interface of Fcα (10, 11) and preferably forms 2:1 complex with a single Fcα homodimer (12). It has been reported that FcγRs and FcϵRI use their membrane proximal-domain and linker region binds immunoglobulin (8, 9, 13, 14), whereas FcαRI uses its membrane-distal domain EC1 to bind IgA (15).

The genes of most FcRs are located in chromosome 1 at 1q21–23 (16), whereas FcαRI is in chromosome 19, at 19q13.4 (17, 18), a region called the leukocyte receptor complex because it is clustered with several leukocyte receptor families including killer cell inhibitory receptors (KIRs) and leukocyte Ig-like receptors (LIR/LILR/ILTs) (17, 18). The amino acid sequence of FcαRI shares only 20% homology with other FcRs, but it has around 35% homology with its neighboring LIRs and KIRs (1).

In this paper, we report our analysis of the crystal structure of the ectodomain of FcαRI expressed in *Escherichia coli* and its comparison with FcRs, LIR, and KIR.

EXPERIMENTAL PROCEDURES

Protein Expression and Purification—The construction and expression of the extracellular ligand binding domain of a human FcαRI will be described in detail elsewhere.[2] Briefly, residues 1–207 of the mature sequence were subcloned into a Novagen pET-28a vector using the *Nco*I and *Xho*I restriction sites and an *E. coli* BL21(DE3) strain. Two additional amino acids (Met-Ala) were added to the 5′ end of the gene, and a histidine tag (His_6) was added to the 3′ end to facilitate the expression and purification. The protein was first expressed in an inclusion body form and then reconstituted *in vitro*. The isolation of the inclusion bodies was started with an intense combined lysozyme/sonification procedure to open virtually all cells. Subsequent washing steps with Triton X-100 and NaCl yielded a product with a purity of >80% as estimated by SDS-PAGE. The

* This work was supported by grants from the National Natural Science Foundation of China (No. C0302050102), Natural Science Foundation of Beijing (No. 7012026), Project "863" (No. 2001AA233011) and Project "973" (No. G1999075600 and No. 200213A711A12). The costs of publication of this article were defrayed in part by the payment of page charges. This article must therefore be hereby marked "*advertisement*" in accordance with 18 U.S.C. Section 1734 solely to indicate this fact.

The atomic coordinates and structure factors (code 1UCT) have been deposited in the Protein Data Bank, Research Collaboratory for Structural Bioinformatics, Rutgers University, New Brunswick, NJ (http://www.rcsb.org/).

¶ These authors contributed equally to this work.

‡‡ To whom correspondence may be addressed. Tel.: 86-10-65221947; Fax: 86-10-65284074; E-mail: wzhang@pumc.edu.cn.

§§ To whom correspondence may be addressed. Tel.: 86-10-62771493; Fax: 86-10-62773145; E-mail: raozh@xtal.tsinghua.edu.cn.

[1] The abbreviations used are: FcR, Fc receptor; KIR, killer cell inhibitory receptor; LIR, leukocyte Ig-like receptor; r.m.s.d., root mean square deviation.

[2] M. Yang, G. Xu, L. Sun, N. Shi, W. Zeng, W. Zhang, and Z. Rao, unpublished data.

inclusion bodies were dissolved in a buffer containing 6 M guanidine hydrochloride and 5 mM dithiothreitol, and incubated for 2 h to unfold completely the misfolded protein of inclusion bodies. Refolding was achieved by dilution of the guanidine-dissolved inclusion bodies dropwise with stirring into the refolding buffer (0.1 M Tris/HCl, 1.5 M guanidine hydrochloride, 5 mM reduced glutathione, 0.5 mM oxidized glutathione, pH 8.5) at 4 °C. The mixture was stirred for 2–3 days, and then the renatured FcαRI was applied to a Q-Sepharose high performance ion-exchange column and further purified on a Superdex-75 column.

Crystallization, Data Collection, and Structure Determination—The FcαRI crystals were obtained by the hanging-drop method. The crystals were grown from a buffer of 11.4% polyethylene glycol-8000 in 100 mM sodium Hepes buffer, pH 7.6, containing 8% (v/v) ethanol glycol, 3% (v/v) Me_2SO, and 50 mM $MgCl_2$ as an additive, and protein concentration of ~12 mg/ml. The Se-Met derivative crystal was grown from the same conditions. The Se-Met derivative data were collected at the Spring8 beamline BL41XU under 100 K at wavelengths 0.9798 Å, 0.9800, and 0.9000 Å and processed using HKL2000 (19). The crystals belong to the space group $C222_1$ with the unit cell dimensions of a = 59.0, b = 69.5, c = 106.4 Å and one molecule in each asymmetric unit. The SOLVE program (20) was used to locate Se sites and to calculate initial phases. Following density modification by RESOLVE (21), the resultant electron density map was of sufficient quality that the entire model except for one flexible loop and several residues at the termini could be built. The initial chain tracing and all subsequent model building were done using the program O (22), version 8.0. Refinement was performed using CNS1.0 (23) and merged synchrotron data with $F_{obs} > 0$. The Bijvoet pairs of the data used in refinement are unmerged. The model was initially refined as a rigid body with data 8.0–4.0 Å resolution. The resolution was extended gradually, and subsequent refinement used protocols including anisotropic temperature factor refinement, energy minimization, and slow cool simulated annealing. Several rounds of manual refitting using omit maps permitted the missing loop regions to be traced and side chains built. 68 water molecules were built into the electron density when a $F_o - F_c$ map, contoured at 3.5σ, coincided with well defined electron density of a $2F_o - F_c$ map contoured at 1σ. The N-terminal 2 additional residues (MA), C-terminal 15 residues (DSIHQDYTTQNLILE), and residues 56–59 (FWNE) were disordered in the crystal. The final model contained 191 residues of FcαRI and 68 solvent molecules. R_{cryst} and R_{free} were 0.210 and 0.239, respectively, for data in the resolution range 40.0–2.1 Å. The structure contains two *cis* prolines at position 154 and 161. None of the main-chain torsion angles are located in disallowed regions of the Ramachandran plot. Statistics for data collection, phasing, and refinement are shown in Table I.

For analyses of interdomain angles, contacts, and buried surface areas, D1 was defined as residues 1–100 and D2 was defined as residues 101–195, following the structure-based definition of KIR2DL1 domain boundaries (24). Interdomain contact residues were defined as being within 3.6 Å of the partner domain and identified using CONTACT (35). Buried surface areas were calculated using SURFACE (35) with a 1.4-Å probe radius.

TABLE I

Data collection, phasing, and refinement statistics

$R_{merge} = \Sigma|I_i - \langle I\rangle|/\Sigma|I|$, where I_i is the intensity of an individual reflection and $\langle I\rangle$ *is the average intensity of that reflection.* R-factor = $\Sigma||F_p| - |F_c||/\Sigma|F_p|$, where F_c is the calculated and F_p is the observed structure factor amplitude. Phasing power = F_{hcalc}/E, where F_{hcalc} = the heavy atom structure factor amplitude and E = the residual lack of closure error. $R_{cullis} = \Sigma||F_{ph} \pm F_p| - |F_{hcalc}||/\Sigma|F_{ph} \pm P_p|$, where F_{ph} is the derivative structure factor amplitude.

Data collection	λ_1 (remote)	λ_2 (peak)	λ_3 (edge)
Wavelength (Å)	0.9000	0.9798	0.9800
Resolution range (Å)	50/2.1	50/2.1	50/2.1
Completeness (%)	100.0 (99.9)	100.0 (99.9)	99.9 (99.5)
Total reflections	95,489	95,646	95,900
Unique reflections	13,108	13,117	13,133
R_{merge} (%)	6.1 (23.4)	6.8 (20.7)	5.2 (18.9)
$I/\sigma(I)$	15.2 (6.7)	15.9 (7.4)	16.2 (7.7)
Redundancy	7.3 (7.0)	7.3 (7.1)	7.3 (7.1)
f'/f'' (electrons)	−1.6/3.3	−7/7	−12/2

Phasing	λ_1 (remote)	λ_2 (peak)	λ_3 (edge)
R_{cullis}			
Centrics	0.75	0.69	0.71
Acentrics (dispersive/anomalous)	0.80/0.77	0.72/0.69	0.73/0.70
Dispersive phasing power (centrics/acentrics)	−/−	1.55/1.89	1.44/1.57
Anomalous phasing power	1.14	1.84	1.66
Figure of merit		0.57	

Refinement	
Total number of reflections used	23,787
Number of reflections in working set	21,565
Number of reflections in test set	2222
Resolution range (Å)	40.0–2.1
Amino acids	195
Water molecules	68
R-factor (%), work	21.0
R-factor (%), free	23.9
r.m.s.d. bonds (Å)	0.015
r.m.s.d. angles (°)	1.8

RESULTS AND DISCUSSION

The crystal structure of the extracellular region of FcαRI consists of two Ig-like domains, EC1 (residues Gln^1 to Gly^{100}) and EC2 (residues Pro^{105} to His^{199}) (Fig. 1*a*). EC1 and EC2 obey the typical heart-shaped arrangement, and a short linker (Leu^{101} to Lys^{104}) connects them together. Both domains are primarily composed of β-structure arranged into two antiparallel β sheets with a KIR-like folding topology. The sheets are closely packed against each other with the conserved disulfide bridge connecting the strands B and F on the opposing sheets. Three 3_{10} helices are found in N termini of EC1 (Glu^2 to Asp^4), EF loops of EC1 (Ala^{71}, Asn^{72}, and Lys^{73}) and EC2 (Leu^{164}, Asn^{165}, and Val^{166}), respectively.

In the EC1 domain, four anti-parallel β-strands (A, B, E, D) oppose a sheet of five β-strands (C′, C, F, G, A′) (Fig. 1*b*). There is a β-bulge (Ser^{91} to Thr^{93}) in the G strand of EC1 splitting the strand into two short β-strands.

The EC2 domain is built up from eight β-strands arranged such that three stands (A, B, E) form one β-sheet and five strands (C′, C, F, G, A′) form a second β-sheet. EC2 does not have a strand in the corresponding position to strand D of EC1. Three residues (Tyr^{181}, Leu^{182}, and Trp^{183}) on EC2 F-G loop stick out. Two of them (Tyr^{181} and Trp^{183}) form hydrogen bonds with Val^{98} on EC1 and the OH group of the side chain of Tyr^{181} forms another hydrogen bond with the side chain of Glu^{95}. Furthermore, Trp^{183} forms hydrogen bonds with Gly^{100} on the end of EC1 and Leu^{101} on the linker.

The interdomain angle of EC1 and EC2 is calculated to be 85°. The bent shape of the FcαRI produces a large interface between the D1D2 domains that buries 1134 $Å^2$ of the accessible surface area (Fig. 1*c*). Most of the residues involved in the EC1 and EC2 interdomain interaction are hydrophobic, including Val^{17} on EC1 A' strand, Ala^{74} and Gly^{75} on EC1 E-F loop, Val^{97}, Val^{98}, Thr^{99}, and Gly^{100} on EC1 G strand, Leu^{101} and Tyr^{102} on the linker strand and Tyr^{173} on EC2 F strand, Tyr^{181} and Trp^{183} on the EC2 F-G loop. The hydrophobic core formed by interactions between these residues stabilizes the interdomain angle. Five of them, namely Val^{17}, Tyr^{97}, Tyr^{173}, Tyr^{181}, and Trp^{183}, are most likely to be important for the conformation. Hydrogen bonds are also found in the hinge region providing additional stability to the hinge angle. These hydrogen bonds (Glu^{95} Oϵ-Tyr^{181} OH, Val^{98} N-Tyr^{181} O, Val^{98} O-Trp^{183} N, Gly^{100} N-Trp^{183} O) mainly involve main-chain atoms and are therefore independent of sequence variation.

As FcαRI shows a relatively high degree of homology to the

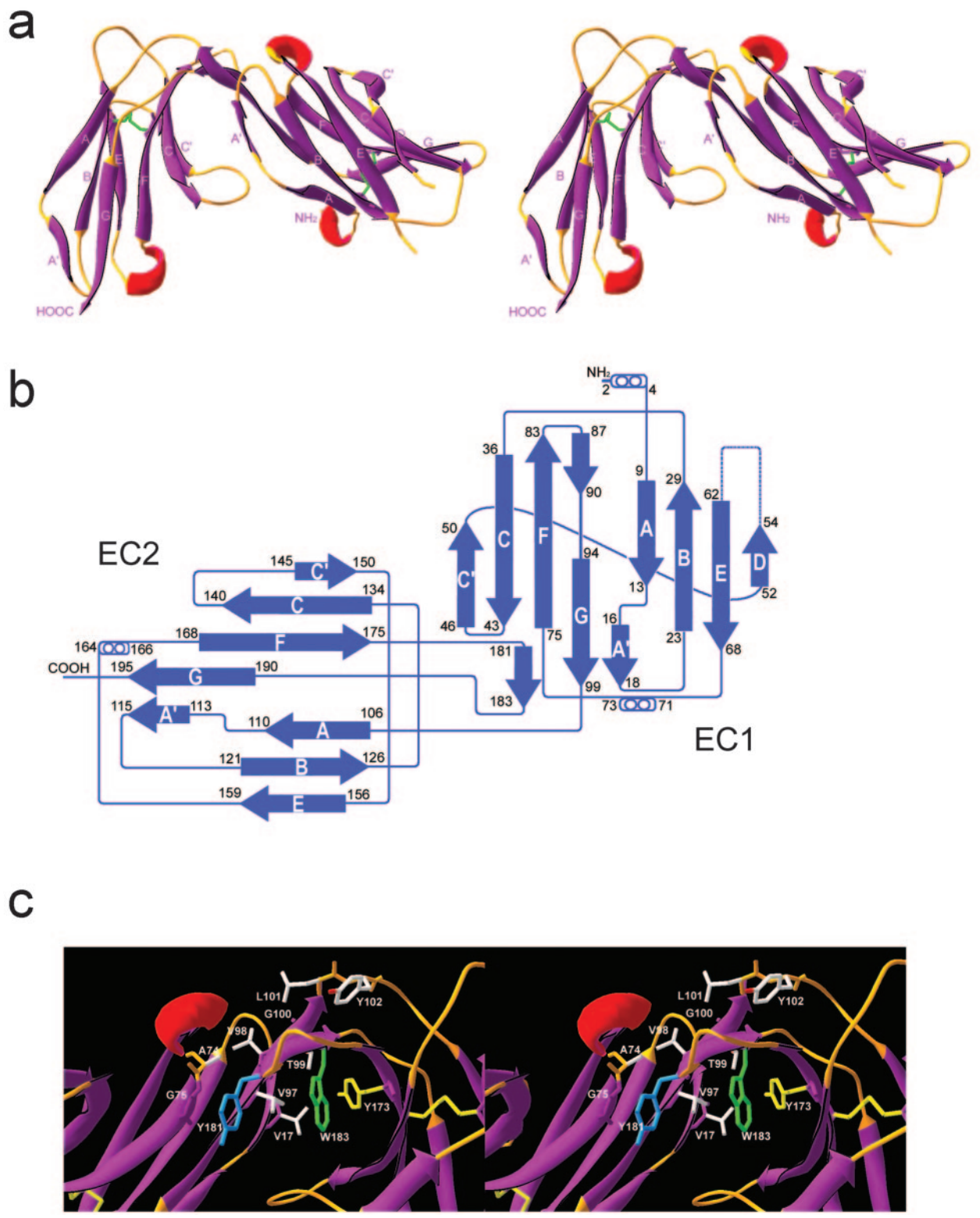

FIG. 1. **Crystal structure of FcαRI ectodomain.** *a*, stereo ribbon drawing of the structure of FcαRI. EC1 is the N-terminal domain, and EC2 is the C-terminal domain. Disulfide bonds are shown in *green*. The residues 56–59 and 196–199 were disordered in the electron density map. *b*, topological diagram of the ectodomain of FcαRI. The *arrows* show the directions of β-strands, whereas the 3_{10} helix structures are represented by *two circles*. The amino acid residues at each end of β-strands and helices are numbered. *c*, close-up stereo view of the hydrophobic core in the interdomain interface of FcαRI. The 12 residues responsible for stabilizing the hydrophobic core are shown in *ball-and-stick* representation. Tyr^{173} (*Y173*) is colored *yellow*, Tyr^{181} (*Y181*) blue, and Trp^{183} (*W183*) *green*. Other residues are colored using the CPK (Corey-Pauling-Kendrew) convention (*blue*, nitrogen; *red*, oxygen; *gray*, carbon; *yellow*, sulfur) color scheme.

D1 and D2 domains of KIR and LIR, the Cα atoms of these three receptors were superimposed to analyze their structural similarities. As shown in Fig. 2*a*, the overall structures of the three receptors are similar especially for the EC2 and D2 domains. The major difference is found in the corresponding position of EC1 C, C′, and D strands of FcαRI. In LIR-1 D1, strands C′ and D are replaced by two 3_{10} helices. On the other hand, the C′ strand of FcαRI is shorter than that of KIR2DL1

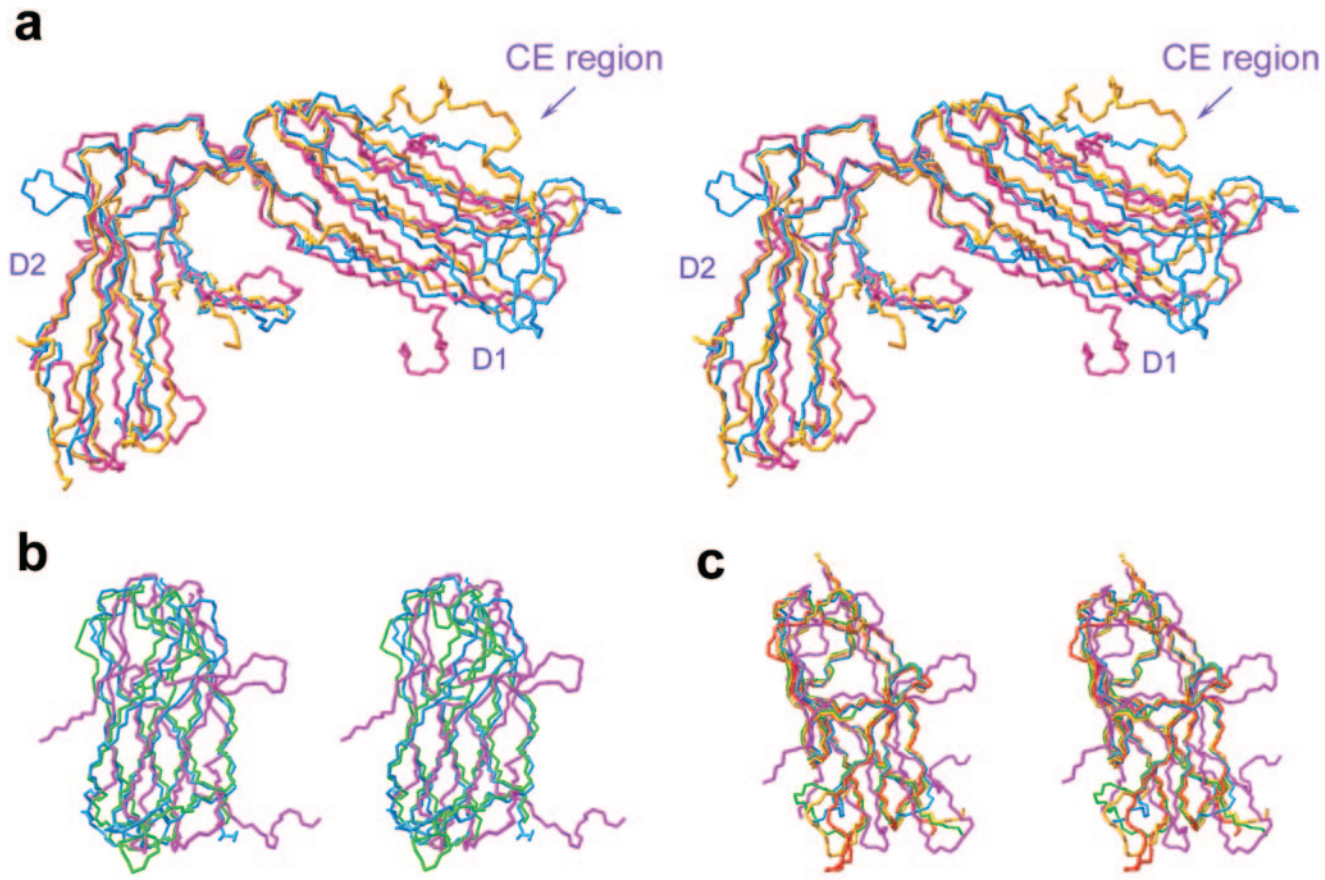

FIG. 2. **Stereo view of the comparison of FcαRI with LIR, KIRs, and FcRs.** *a*, superimpose of FcαRI (*purple*), LIR-1 (*orange*), and KIR2DL2 (*blue*). The r.m.s.d. values for superimposition are: 1.44 Å for FcαRI EC1 and LIR-1 D1, 1.54 Å for FcαRI EC1 and KIR2DL2 D1, 1.34 Å for FcαRI EC2 and LIR-1 D2, and 1.18 Å for FcαRI EC2 and KIR2DL2 D2. *b*, comparison of EC1 CC′ loop of FcαRI with KIR2DL1 and KIR2DL2. The Cα trace of FcαRI is colored *purple*, KIR2DL1 is in *green*, and KIR2DL2 is in *blue*. *c*, comparison of EC1 C to E region of FcαRI with other human FcR structures. The Cα traces of FcαRI, FcεRI, FcγRIIa, FcγRIIb, and FcγRIII are colored *purple*, *blue*, *orange*, *green*, and *red*, respectively.

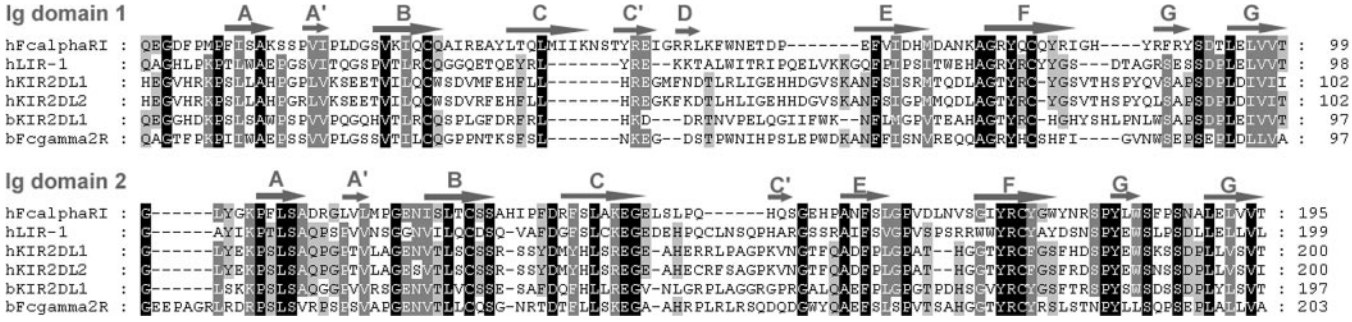

FIG. 3. **Comparison of the sequences of human FcαRI with human LIR-1, human KIR2DL1, human KIR2DL2, bovine KIR2DL1, and bovine FcαIIR.** The secondary β-strands of FcαRI are shown above the sequence with *bold arrows*. Conserved residues are *shaded*. Deletions in the sequences are indicated by *dashes*.

and KIR2DL2. Hence, the C-C′ loop in FcαRI EC1 forms earlier (Fig. 2*b*), allowing the C-C′ loop and F-G loop to adopt a clamp-like arrangement. A similar feature can also be found in many other FcRs (Fig. 2*c*) even though they share low degree of identity with FcαRI. The significance of this is still unknown.

Although LIR-1 does not contain of C′ and D strands in the D1 domain, it more closely resembles FcαRI in the other part of the molecule compared with KIR2DL1 and KIR2DL2. The root mean square deviation (r.m.s.d) values for the Cα atoms are 1.44 Å for FcαRI EC1 and LIR-1 D1, 1.54 Å for FcαRI EC1 and KIR2DL2 D1 and 1.77 Å for FcαRI EC1 and KIR2DL1 D1. It seems the lack of C′ and D strands in LIR-1 D1 have little effect on its overall structure, although the sequence of C′ and D regions are variable within KIR2DL1, KIR2DL2, and LIR-1 (Fig. 3).

The interdomain angle of FcαRI is closer to that of LIR-1 (84 to 90°) (25), but larger than that of KIR2DL2 (60 to 80°) (26). The hydrophobic core interface observed in FcαRI also exists in LIR-1 and KIR2DL2 (25, 26). Amino acid sequence alignment shows the 12 hydrophobic residues, especially Tyr^{181} and Trp^{183}, which play an important role in stabilizing the interdomain angle in FcαRI are also conserved in LIR-1 and KIRs, having only one residue (Leu^{101} → Ala) different for LIR-1, three residues (Val^{17} → Leu, Val^{98} → Ile, and Tyr^{173} → Phe) different for KIR2DL2 and four residues (Val^{17} → Leu, Val^{98} → Ile, Thr^{99} → Ile and Tyr^{173} → Phe) different for KIR2DL1. These 12 residues are also conserved in a KIR from cow, with only one residue (Tyr^{102} → Ser) different from FcαRI in this region (Fig. 3). Moreover, a bovine IgG2 FcR, Fcγ2R, also possesses most of these hydrophobic residues and only four

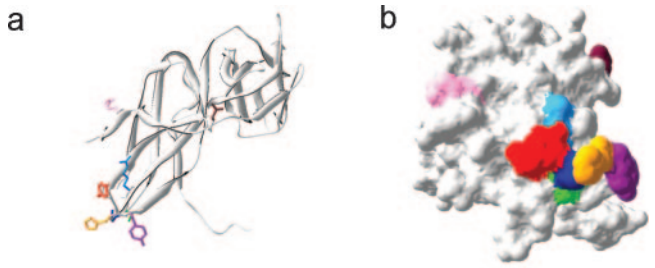

FIG. 4. **Residues involved in FcαRI binding of IgA.** *a*, position of the potential binding area on FcαRI. *b*, molecular surface of FcαRI. The residues involved in binding of IgA are highlighted in color. Tyr^{35} is colored *red*, Asn^{44} *brown*, Arg^{52} *pink*, Arg^{82} *blue*, Ile^{83} *green*, Gly^{84} *dark blue*, His^{85} *orange*, and Tyr^{87} *purple*. The structure was represented by DeepView Swiss-PdbViewer (34).

residues (Val^{97} → Leu, Thr^{99} → Ala and Tyr^{102} → Arg and Trp^{183} → Leu) are different from FcαRI. This Fcγ2R has been previously found to share more similarities to FcαRI (41%) than to other types of human FcγRs (less than 28%) (27), and it is located on the same chromosome as bovine KIR (28, 29), indicating that it belongs to the bovine leukocyte receptor complex. In contrast, such a hydrophobic core does not exist in human FcRs for IgG and IgE (11, 30–33). This suggests that the hydrophobic core is a common feature of receptors from the leukocyte receptor complex and FcαRI is evolutionally closer to LIR and KIR than to other human FcRs.

As an immunoglobulin Fc receptor, FcαRI differs from other FcRs not only in structure but also in its ligand binding characteristics. IgG receptor FcγRIII and IgE receptor FcεRI bind antibodies in the near hinge regions and form 1:1 complexes (8, 9). In contrast, FcαRI binds the C_H2-C_H3 interface of Fcα (10, 11) and preferably forms a 2:1 complex with a single Fcα homodimer (12). It has been reported that FcγRs and FcεRI use their membrane-proximal domain and linker region to bind immunoglobulin (8, 9, 13, 14), whereas FcαRI uses its membrane-distal domain EC1 to bind IgA (33). A number of residues have been implicated in IgA binding, including Tyr^{35}, Arg^{52}, Tyr^{81}, Arg^{82}, Ile^{83}, Gly^{84}, His^{85}, and Tyr^{86} (6). The crystal structure of FcαRI shows that Tyr^{35} is located in the B-C loop, Arg^{52} is located in C′ strand, Tyr^{81} and Arg^{82} are located in F strand, and the remainder are in the F-G loop. All these residues lie on the receptor surface except Tyr^{81}, which is buried inside the receptor and is unlikely to be involved directly in IgA binding (Fig. 4).

FcαRI has six potential *N*-linked glycosylation sites (Asn^{44}, Asn^{58}, Asn^{120}, Asn^{156}, Asn^{165}, and Asn^{177}). Unglycosylated FcαRI has a molecular mass of 30 kDa. When expressed *in vivo*, its molecular mass is increased to 50–100 kDa due to different degrees of glycosylation (1). Although the effect of glycosylation still needs to be elucidated, carbohydrates seem to play an important role in IgA binding since desialylated FcαRI binds five times more strongly to IgA (1). Fig. 4 shows the position of potential *N*-linked glycosylation site at Asn^{44}, which is close to the docking sites of IgA.

In conclusion, the crystal structure and sequence alignment show that FcαRI is a member of the leukocyte receptor complex and evolutionally closer to LIR than KIR. All members of this complex found so far share a common hydrophobic core structure. The crystal structure also locates the residues that are involved in FcαRI binding to IgA.

Acknowledgments—We thank Fei Sun, Feng Xu, and Zhiyong Lou for assistance with data collection at Spring-8 BEAMLINE BL41XU. We also thank Drs. Mark Bartlam and Yiwei Liu for valuable discussion and reading of the manuscript.

REFERENCES

1. Monteiro, R. C., and van De Winkel, J. G. (2003) *Annu. Rev. Immunol.* **21,** 177–204
2. Kerr, M. A. (1990) *Biochem. J.* **271,** 285–296
3. Galla, J. H. (1995) *Kidney Int.* **47,** 377–387
4. Maliszewski, C. R., March, C. J., Schoenborn, M. A., Gimpel, S., and Shen, L. (1990) *J. Exp. Med.* **172,** 1665–1672
5. Mazengera, R. L., and Kerr, M. A. (1990) *Biochem. J.* **272,** 159–165
6. Wines, B. D., Sardjono, C. T., Trist, H. H., Lay, C. S., and Hogarth, P. M. (2001) *J. Immunol.* **166,** 1781–1789
7. Wines, B. D., Hulett, M. D., Jamieson, G. P., Trist, H. M., Spratt, J. M., and Hogarth, P. M. (1999) *J. Immunol.* **162,** 2146–2153
8. Sondermann, P., Huber, R., Oosthuizen, V., and Jacob, U. (2000) *Nature* **406,** 267–273
9. Garman, S. C., Wurzburg, B. A., Tarchevskaya, S. S., Kinet, J. P., and Jardetzky, T. S. (2000) *Nature* **406,** 259–266
10. Carayannopoulos, L., Hexham, J. M., and Capra, J. D. (1996) *J. Exp. Med.* **183,** 1579–1586
11. Pleass, R. J., Dunlop, J. I., Anderson, C. M., and Woof, J. M. (1999) *J. Biol. Chem.* **274,** 23508–23514
12. Herr, A. B., White, C. L., Milburn, C., Wu, C., and Bjorkman, P. J. (2003) *J. Mol. Biol.* **327,** 645–657
13. Sondermann, P., and Oosthuizen, V. (2002) *Biochem. Soc. Trans.* **30,** 481–486
14. Hulett, M. D., and Hogarth, P. M. (1998) *Mol. Immunol.* **35,** 989–996
15. Morton, H. C., van Zandbergen, G., van Kooten, C., Howard, C. J., van de Winkel, J. G., and Brandtzaeg, P. (1999) *J. Exp. Med.* **189,** 1715–1722
16. Davis, R. S., Dennis, G., Jr., Odom, M. R., Gibson, A. W., Kimberly, R. P., Burrows, P. D., and Cooper, M. D. (2002) *Immunol. Rev.* **190,** 123–136
17. Kremer, E. J., Kalatzis, V., Baker, E., Callen, D. F., Sutherland, G. R., and Maliszewski, C. R. (1992) *Hum. Genet.* **89,** 107–108
18. Volz, A., Wende, H., Laun, K., and Ziegler, A. (2001) *Immunol. Rev.* **181,** 39–51
19. Otwinowski, Z., and Minor, W. (1997) *Macromol. Crystallogr. Part A* **276,** 307–326
20. Terwilliger, T. C., and Berendzen, J. (1999) *Acta Crystallgr. Sect. D Biol. Crystallogr.* **55,** 849–861
21. Terwilliger, T. C. (2001) *Acta Crystallogr. Sect. D Biol. Crystallogr.* **57,** 1755–1762
22. Jones, T. A., Zou, J. Y., Cowan, S. W., and Kjeldgaard, M. (1991) *Acta Crystallogr. Sect. A* **47,** 110–119
23. Brunger, A. T., Adams, P. D., Clore, G. M., DeLano, W. L., Gros, P., Grosse-Kunstleve, R. W., Jiang, J. S., Kuszewski, J., Nilges, M., Pannu, N. S., Read, R. J., Rice, L. M., Simonson, T., and Warren, G. L. (1998) *Acta Crystallogr. Sect. D Biol. Crystallogr.* **54,** 905–921
24. Fan, Q. R., Mosyak, L., Winter, C. C., Wagtmann, N., Long, E. O., and Wiley, D. C. (1997) *Nature* **389,** 96–100
25. Chapman, T. L., Heikema, A. P., West, A. P. Jr., and Bjorkman, P. J. (2000) *Immunity* **13,** 727–736
26. Snyder, G. A., Brooks, A. G., and Sun, P. D. (1999) *Proc. Natl. Acad. Sci. U. S. A.* **96,** 3864–3869
27. Zhang, G., Young, J. R., Tregaskes, C. A., Sopp, P., and Howard, C. J. (1995) *J. Immunol.* **155,** 1534–1541
28. Storset, A. K., Slettedal, I. O., Williams, J. L., Law, A., and Dissen, E. (2003) *Eur. J. Immunol.* **33,** 980–990
29. Klungland, H., Vage, D. I., and Lien, S. (1997) *Mamm. Genome* **8,** 300–301
30. Garman, S. C., Kinet, J. P., and Jardetzky, T. S. (1998) *Cell* **95,** 951–961
31. Powell, M. S., Barton, P. A., Emmanouilidis, D., Wines, B. D., Neumann, G. M., Peitersz, G. A., Maxwell, K. F., Garrett, T. P., and Hogarth, P. M. (1999) *Immunol. Lett.* **68,** 17–23
32. Maxwell, K. F., Powell, M. S., Hulett, M. D., Barton, P. A., McKenzie, I. F., Garrett, T. P., and Hogarth, P. M. (1999) *Nat. Struct. Biol.* **6,** 437–442
33. Sondermann, P., Huber, R., and Jacob, U. (1999) *EMBO J.* **18,** 1095–1103
34. Guex, N., and Peitsch, M. C. (1997) *Electrophoresis* **18,** 2714–2723
35. Collaborative Computational Project, Number 4 (1994) *Acta Crystallogr. Sect. D Biol. Crystallogr.* **50,** 760–763